Frontiers of Physics
https://doi.org/10.1007/s11467-021-1088-3
Front. Phys.
16(6), 63506 (2021)

RESEARCH ARTICLE

Diverse magnetism in stable and metastable structures of CrTe

Na Kang, Wenhui Wan†, Yanfeng Ge, Yong Liu‡

State Key Laboratory of Metastable Materials Science and Technology & Key Laboratory for Microstructural Material Physics of Hebei Province, School of Science, Yanshan University, Qinhuangdao 066004, China

Corresponding authors. E-mail: †wwh@ysu.edu.cn, ‡yongliu@ysu.edu.cn

Received January 2, 2021; accepted May 12, 2021

SUPPLEMENTARY MATERIAL

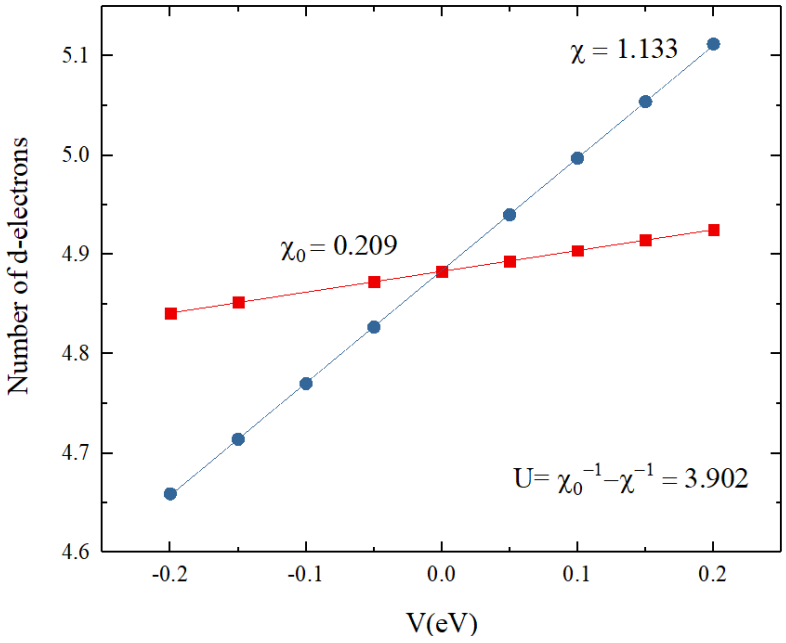

Fig. S1 Estimation of U_f of CrTe, according to linear response method by Cococcioni *et al.* [*Phys. Rev. B* 71, 035105 (2005)], the effective U is calculated by

$$U = \chi_0^{-1} - \chi^{-1} \approx \left(\frac{\partial N_I^{NSCF}}{\partial V_I}\right)^{-1} - \left(\frac{\partial N_I^{SCF}}{\partial V_I}\right)^{-1}$$

where N_I is the projected charge number of d-electrons of *I-th* Cr atom in self-consistent (SCF) calculation or non-self-consistent (NSCF) calculations. V is the potential shift used. The calculated U_f of Cmca phase is 3.902 eV. With similar process, the U_f of $P6_3/mmc$, $R\bar{3}m$ and $Fm\bar{3}m$ phase are between 4.0−5.0 eV. Thus, we adopted U_f = 4.0 eV for all the CrTe structures for comparing their energy with each other.

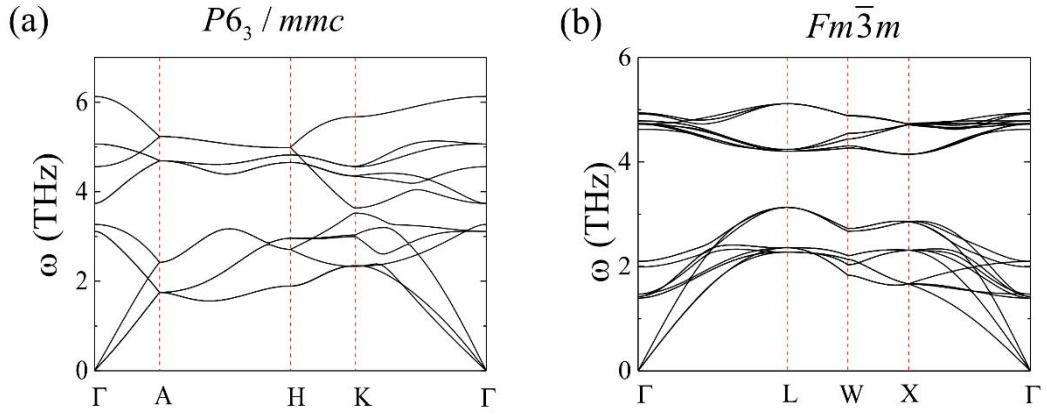

Fig. S2 The phonon dispersion of CrTe in **(a)** $P6_3/mmc$ (NA) and **(b)** $Fm\bar{3}m$ (RS) structures.

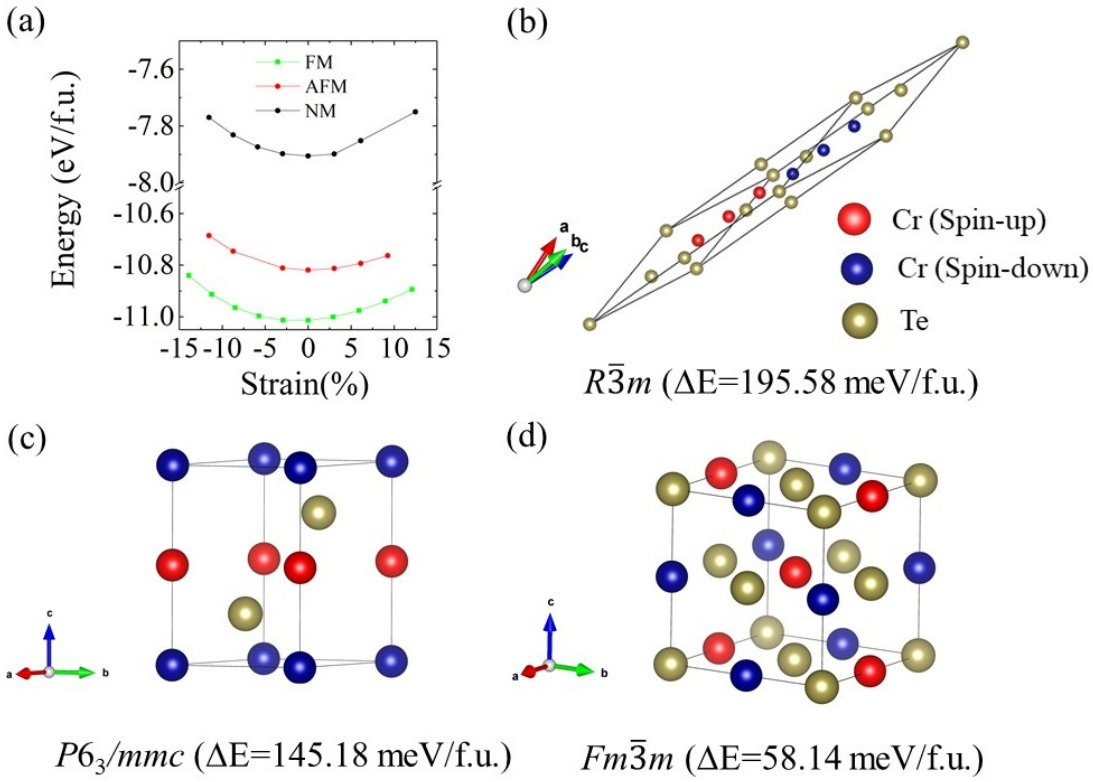

Fig. S3 (a) The energy-volume curve of CrTe in $R\bar{3}m$ structures. The FM state has the lowest energy. The meta-stable antiferromagnetic configurations of CrTe in **(b)** $R\bar{3}m$, **(c)** $P6_3/mmc$, **(d)** $Fm\bar{3}$ structures. $\Delta E = E_{AFM} - E_{FM}$ indicates the energy difference between the meta-stable antiferromagnetic state and ground-state ferromagnetic state. The above antiferromagnetic states were picked out with the lowest energy among various AFM states. The red and blue balls indicate the Cr atom with up and down spin, respectively.

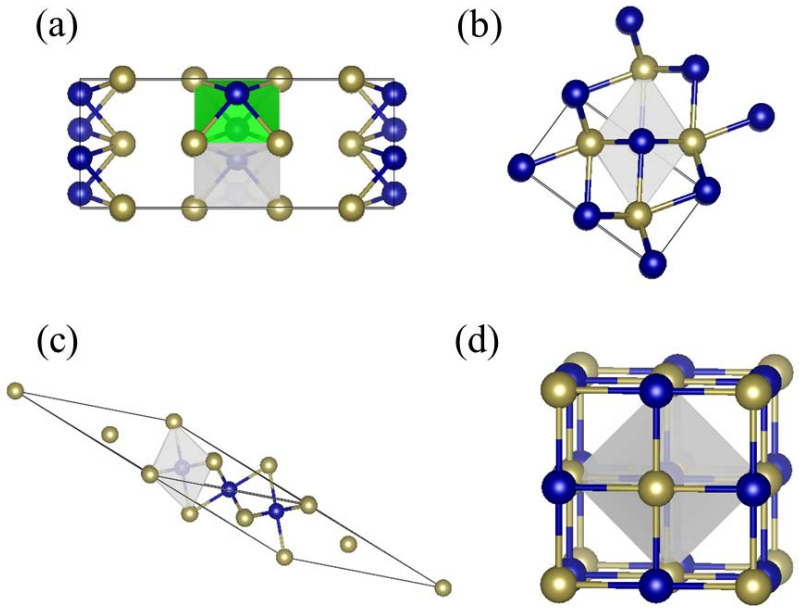

Fig. S4 The crystal structure of CrTe in **(a)** *Cmca* **(b)** $P6_3/mmc$, **(c)** $R\bar{3}m$ and **(d)** $Fm\bar{3}m$ structures with basic unit displayed. The basic unit of *Cmca* and the other three structures are the quadrangular and octahedron, respectively.

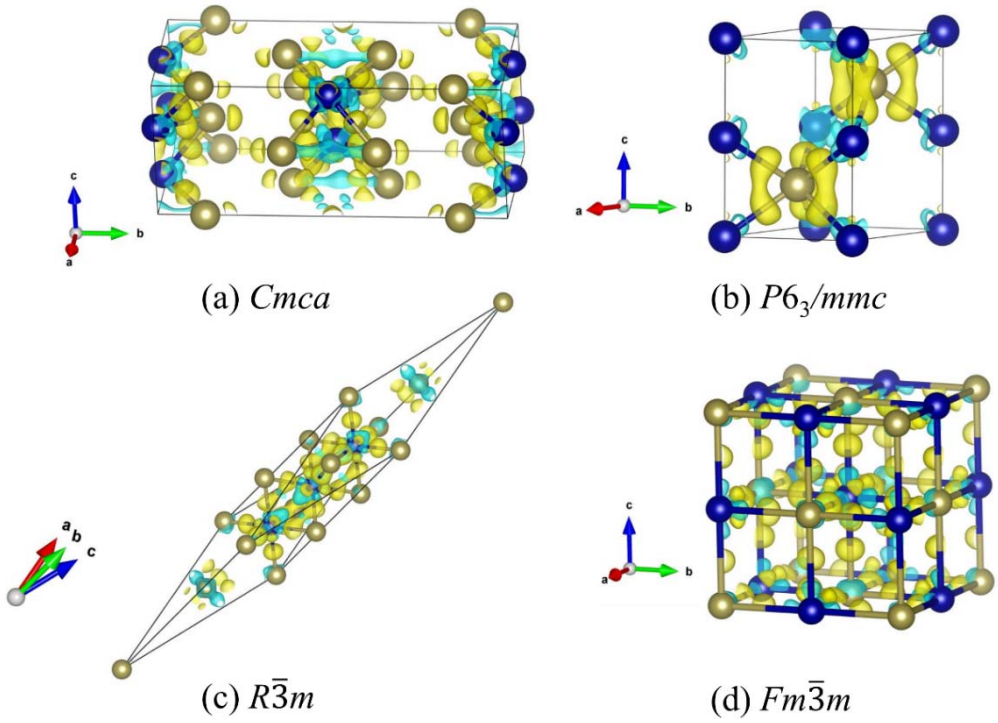

Fig. S5 The charge density difference of CrTe in **(a)** *Cmca*, **(b)** $P6_3/mmc$, **(c)** $R\bar{3}m$ and **(d)** $Fm\bar{3}m$ structures.

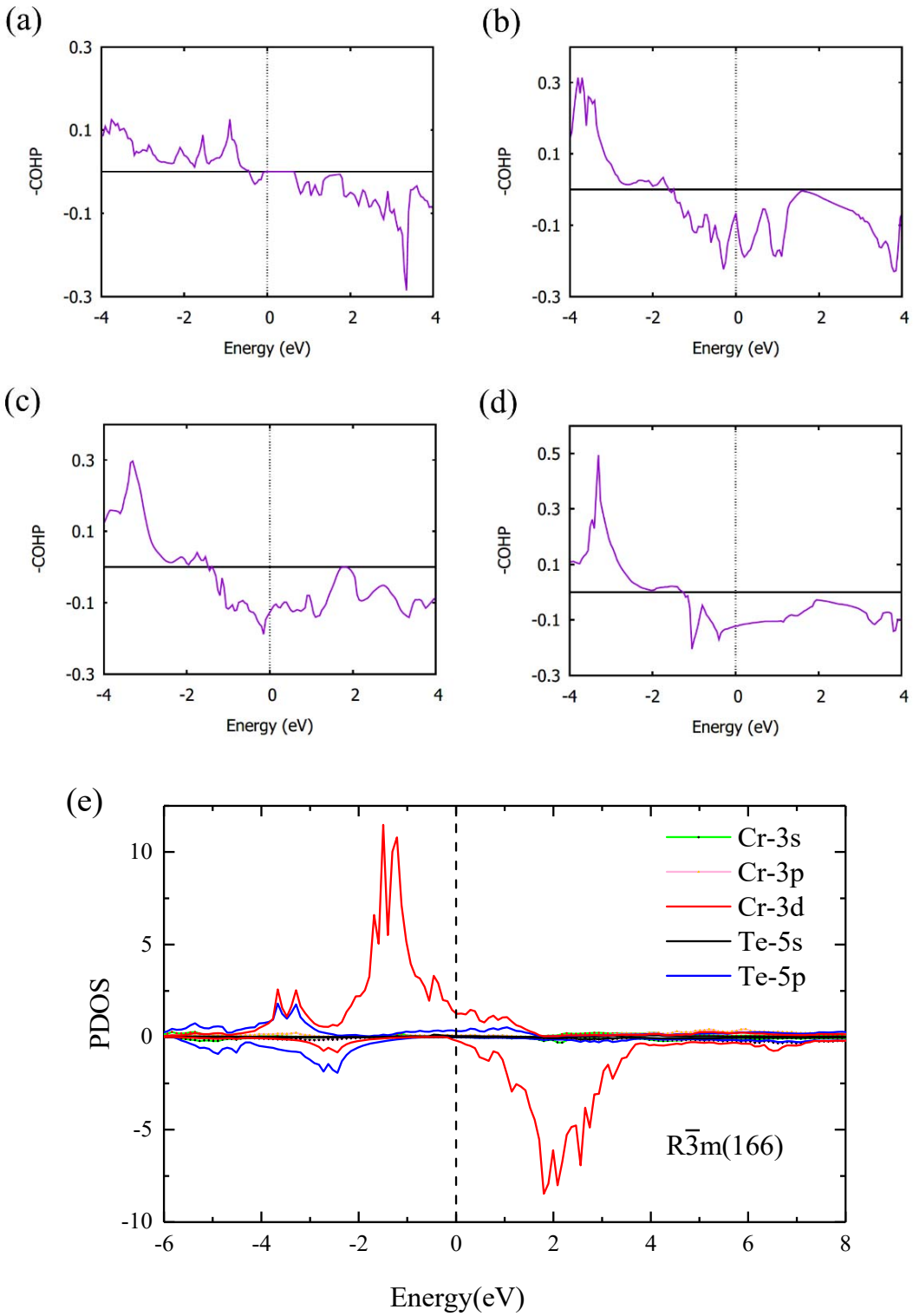

Fig. S6 The crystal orbital Hamilton populations (−COHP) of CrTe in **(a)** *Cmca*, **(b)** *P6₃/mmc*, **(c)** $R\bar{3}m$ and **(d)** $Fm\bar{3}m$ structures. Positive and negative COHP indicates bonding and anti-bonding states, respectively. **(e)** The projected density of states of CrTe in $Fm\bar{3}m$ structures.

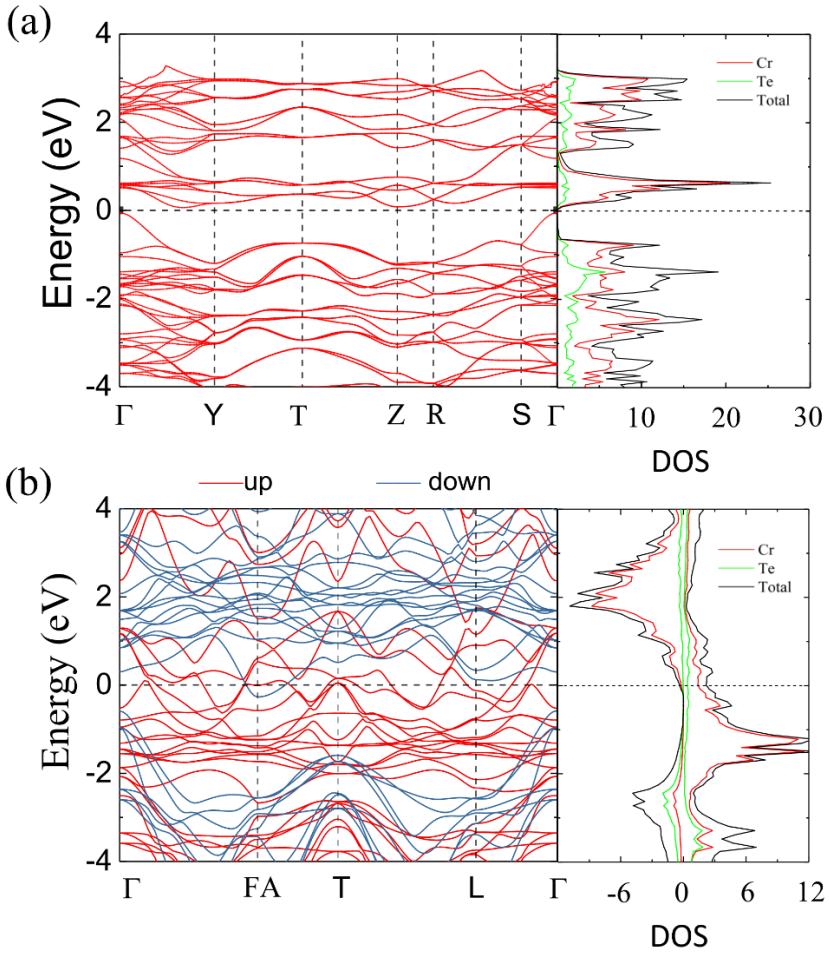

Fig. S7 The band structure of CrTe in **(a)** *Cmca* and **(b)** $R\bar{3}m$ structures with PBE method. Without electron correlation effect considered, *Cmca* structure become an AFM semiconductor with a band gap of 0.126 eV.

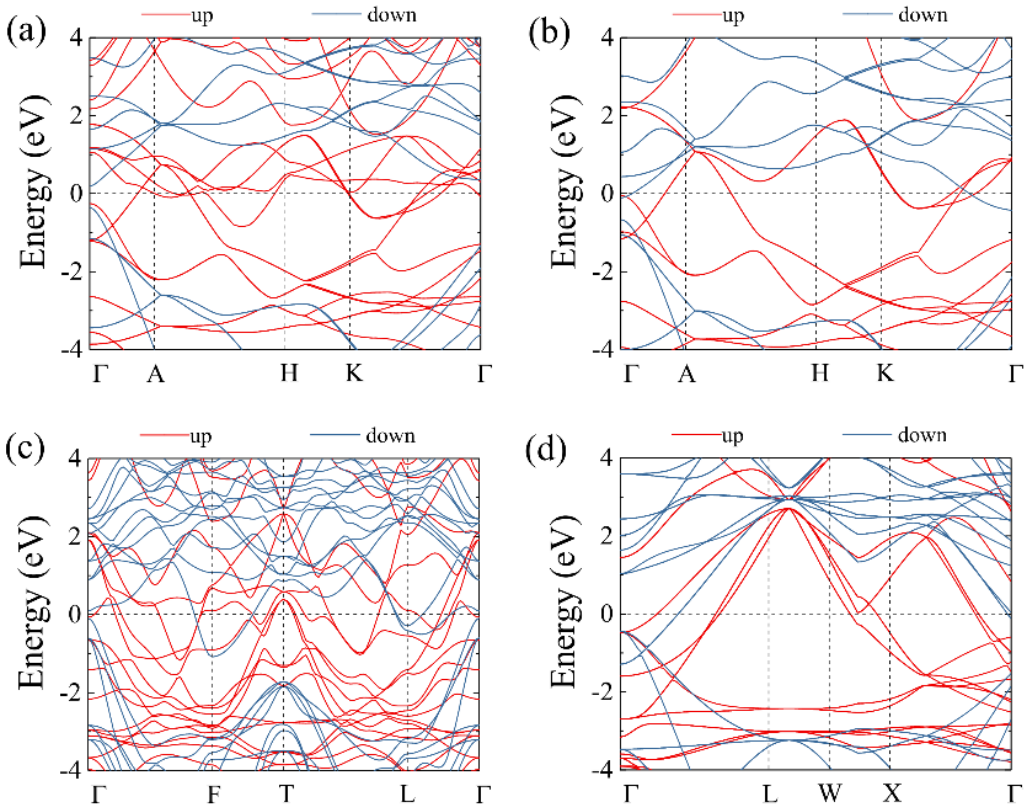

Fig. S8 The band structure of CrTe in **(a)** P6$_3$/mmc structure at 30 Gpa; **(b)** *P*6$_3$/*mmc* structure at 50 Gpa; **(c)** $R\bar{3}m$ structure at 50 Gpa; **(d)** $Fm\bar{3}m$ structure at 50 Gpa.

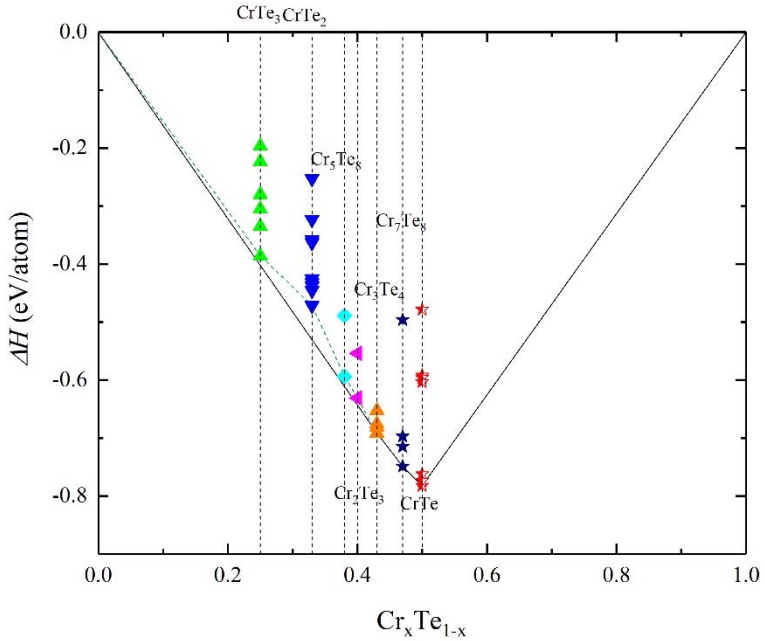

Fig. S9 Calculated formation enthalpies per atom of Cr−Te compounds within the chemical compositions available in the experiment.

Table S1 A table comparing of CrTe belonging to different structures in previous works. The phases of CrTe were sorted by the energy in ascending order. The most stable phases= in each work was labeled. The reference listed in the table can be seen in the main content according to reference number.

Ref.	Calculation method	The considered phases of CrTe
Our work	PAW+PBE	*Cmca* **(most stable)**, $P6_3/mmc$ (NiAs), $R\bar{3}m$, $Fm\bar{3}m$ (RS)
	PAW+PBE+*U* (*U*=4eV)	$P6_3/mmc$ **(**NiAs, **most stable)**, $R\bar{3}m$, $Fm\bar{3}m$ (RS), *Cmca*,
15	FP-LAPW +PBE	NiAs **(most stable)**, RS, ZB
17	TB-LMTO	NiAs **(most stable)**, MnP
18	FP-LAPW +PBE	NiAs **(most stable)**, ZB
20	FP-LAPW +LDA	NiAs **(most stable)**, RS, ZB
21	FP-LAPW +GGA	NaCl **(most stable)**, ZB, WZ, NiAs, CsCl
	FP-LAPW +GGA+*U* (*U* = 4eV)	NaCl **(most stable)**, NiAs, ZB, WZ, CsCl
22	FP-LAPW +GGA+*U* (*U*=0, 2, 4 eV)	ZB **(most stable)**, WZ

Table S2 The independent elastic constant and Born criterion of CrTe structure in hexagonal ($P6_3/mmc$), trigonal ($R\bar{3}m$), cubic ($Fm\bar{3}m$), and orthorhombic ($Cmca$) phases.

Independent elastic constant C_{ij}	Mechanical stability criterion
Hexagonal phase (C_{11}, C_{33}, C_{44}, C_{12} and C_{13})	$C_{44} > 0$ $C_{11} > \lvert C_{12} \rvert$ $(C_{11} + C_{12})C_{33} > 2C_{13}^2$
Trigonal phase (C_{11}, C_{33}, C_{44}, C_{14}, C_{12} and C_{13})	$C_{44} > 0$ $C_{11} > \lvert C_{12} \rvert$ $(C_{11} + C_{12})C_{33} > 2C_{13}^2$ $(C_{11} - C_{12})C_{44} > 2C_{14}^2$
cubic phase (C_{11}, C_{44}, and C_{12})	$C_{11} > 0$ $C_{44} > 0$ $C_{11} > \lvert C_{12} \rvert$ $C_{11} + 2C_{12} > 0$
Orthorhombic phase (C_{11}, C_{22}, C_{33}, C_{44}, C_{55}, C_{66}, C_{12}, C_{13}, and C_{23})	$C_{ii} > 0$ $C_{ii} + C_{jj} - 2C_{ij} > 0$ $C_{11} + C_{22} + C_{33} + 2(C_{12} + C_{13} + C_{23}) > 0$